



Contents lists available at ScienceDirect

# Spectrochimica Acta Part A: Molecular and Biomolecular Spectroscopy

journal homepage: [www.elsevier.com/locate/saa](http://www.elsevier.com/locate/saa)

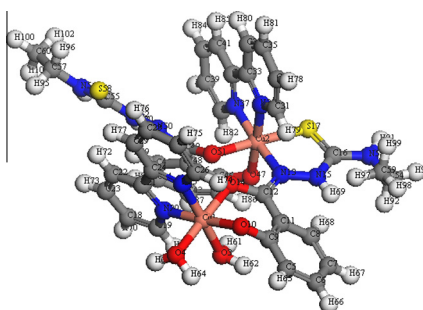
## Comparative studies between 4-allyl-, 4-phenyl- and 4-ethyl-1-(2-hydroxybenzoyl) thiosemicarbazides and the synthesis, characterization and DFT calculations of binary and ternary complexes derived from 4-ethyl ( $L^1$ ) and 2,2'-dipyridyl

Shaker J. Azhari<sup>a</sup>, Mosaad R. Mlahi<sup>b</sup>, Mohsen M. Mostafa<sup>b,\*</sup><sup>a</sup> Chemistry Department, Faculty of Applied Sciences, Umm Al-Qura University, Saudi Arabia<sup>b</sup> Chemistry Department, Faculty of Science, Mansoura University, Mansoura, Egypt

### HIGHLIGHTS

- DFT calculations.
- Binary and ternary complexes.
- Complexes derived from thiosemicarbazide.
- Uncommon geometries of metal complexes.

### GRAPHICAL ABSTRACT



### ARTICLE INFO

#### Article history:

Received 28 October 2014

Received in revised form 15 June 2015

Accepted 17 June 2015

Available online 22 June 2015

#### Keywords:

Comparative studies between 4-allyl-, 4-phenyl- and 4-ethyl-1-(2-hydroxybenzoyl) thiosemicarbazides  
Binary and ternary complexes  
4-Ethyl-1-(2-hydroxybenzoyl)thiosemicarbazide complexes  
Geometries of  $Co^{2+}$ ,  $Cu^{2+}$  complexes  
DFT calculations  
Biological activity

### ABSTRACT

The metal complexes of 4-ethyl-1-(2-hydroxybenzoyl) thiosemicarbazide ( $L^1$ ) with  $MCl_2$  ( $M = Co^{2+}$ ,  $Cu^{2+}$  and  $Zn^{2+}$ ) and  $Zn(Ac)_2$  in EtOH were synthesized and characterized using spectral (IR,  $^1H$ -NMR, mass, UV-Visible), magnetic moment and thermal measurements. Binary and ternary complexes with the general formulae,  $[Cu(L^1-H)_2] \cdot EtOH$ ,  $[Co(L^1-H)_2]$ ,  $[Zn_3(L^1-H)(L^1)(Ac)_5]$ ,  $[Cu_2(L^2)_2(L^1-2H)_2(H_2O)_2] \cdot 4H_2O$ ,  $[Co(L^2)(L^1-2H)] \cdot 3H_2O$  and  $[Zn_2(L^2)(OH)(L^1-3H)(H_2O)] \cdot 1/2EtOH$  where  $L^2$  is 2,2'-dipyridyl, have been suggested and characterized. The bond lengths, bond angles, chemical reactivities, energy components, binding energies and dipole moments for the isolated complexes were evaluated by DFT method from DMOL<sup>3</sup>. Also, the MEP for  $L^1$  is illustrated. The existence of the OH group in the  $Zn^{2+}$  ternary complexes is confirmed by IR, mass and  $^1H$ -NMR spectra. Biological activity for the  $L^1$  and some its complexes was tested against DNA. Comparative studies between the ligation behavior and reactivity of our previous work derived from 4-phenyl- and 4-allyl-1-(2-hydroxybenzoyl) thiosemicarbazides have been investigated.

© 2015 Elsevier B.V. All rights reserved.

## 1. Introduction

Thiosemicarbazides and its derivatives have been raised considerable interest in chemistry and biology [1]. Also, these compounds have different applications such as antiparasite [2], antibacterial

\* Corresponding author.

E-mail address: [amohsenmostafa@yahoo.com](mailto:amohsenmostafa@yahoo.com) (M.M. Mostafa).

[3], antitumor [4,5], antimalarial [6] and antiviral [7]. In continuation of our earlier work [8–14] and others [15–19] and due to the importance of these compounds, we extend this work to include thiosemicarbazide derived from salicylic acid hydrazide. Also, the ternary metal complexes with 2,2'-dipyridyl were synthesized and characterized. The biological activity of **L**<sup>1</sup> and two metal complexes were tested against DNA. Moreover, comparative studies between our previous works of 4-allyl- and 4-phenyl-4-(2-hydroxybenzoyl) thiosemicarbazides [20,21] have been studied. Finally, we focused our attention to study the role and behavior of ethyl, phenyl and/or allyl attached in the 4-position of the thiosemicarbazide moiety on the geometry of complex formation as well as on the reactivity toward DNA.

## 2. Experimental

### 2.1. Instrumentation and materials

All the chemicals were purchased from Aldrich and Fluka and used without further purification. All the methods and instrumentations are described in earlier works [22,23].

### 2.2. Synthesis of synthesis of the ligand (**L**<sup>1</sup>)

4-Ethyl-1-(2-hydroxybenzoyl) thiosemicarbazide (**L**<sup>1</sup>) was synthesized similar to these described earlier in our previous work [20,21] but using ethyl isothiocyanate. **L**<sup>1</sup> was checked by its melting point (217–218 °C) and TLC.

### 2.3. Syntheses of binary metal complexes

A solution of **L**<sup>1</sup> (0.01 mol; 2.5 g) in EtOH was added to the metal salt solutions (0.01 mol) of CoCl<sub>2</sub>·6H<sub>2</sub>O (2.4 g), CuCl<sub>2</sub>·2H<sub>2</sub>O (1.7 g) and Zn(Ac)<sub>2</sub>·2H<sub>2</sub>O (2.2 g) in EtOH (50 mL). The reaction mixtures were refluxed on a hot plate for ~3 h. The pH of the solutions were found in the range 1–2 for the Cu<sup>2+</sup> and Co<sup>2+</sup> complexes while at 5 in case of the Zn<sup>2+</sup> complex.

### 2.4. Syntheses of ternary metal complexes

A solution of 2,2'-dipyridyl (**L**<sup>2</sup>, 0.003 mol; 0.45 g) in EtOH (25 mL) was added to a solution of CoCl<sub>2</sub>·6H<sub>2</sub>O (0.003 mol; 0.72 g), CuCl<sub>2</sub>·2H<sub>2</sub>O (0.003 mol; 0.51 g) and ZnCl<sub>2</sub> (0.003 mol; 0.42 g) in EtOH (25 mL). The binary solid complexes derived from 2,2'-dipyridyl were filtered off and washed with hot EtOH and diethyl ether, respectively. The ternary complexes were synthesized by dissolving the isolated solid complexes derived from 2,2'-dipyridyl in redistilled water (0.003 mol; 0.8 g) in case of the Cu<sup>2+</sup> complex, (0.002 mol; 0.6 g) for the Co<sup>2+</sup> complex and (0.004 mol; 1.2 g) in case of Zn<sup>2+</sup> complex. **L**<sup>1</sup> was dissolved in absolute EtOH (25 mL) and then added to the above complex solutions. The reaction mixtures were heated on a hot plate for 4 h. The

pH of the solution was raised to 5 in case of Co<sup>2+</sup> and Zn<sup>2+</sup> complexes using KOH solution. The Cu<sup>2+</sup> complex was obtained at pH = 2 and without raising the pH of the solution. All the binary and ternary complexes were filtered off, washed several times with hot EtOH and diethyl ether, respectively. The isolated solid complexes were dried in oven at 120 °C for 1.5 h.

### 2.5. Genotoxicity activity

The methodology for studding genotoxicity activity was described earlier [20,21].

## 3. Computational details

All computational calculations using DMOL<sup>3</sup> program are reported in our previous work [20,21].

## 4. Results and discussion

All the isolated metal complexes are colored, insoluble in most common organic solvents but partially soluble in DMSO and DMF, except the Zn<sup>2+</sup> complexes, which are white in color. The value of  $\Lambda_m^+$  for the ternary Zn<sup>2+</sup> complex (5.0 Ω<sup>-1</sup> cm<sup>2</sup> mol<sup>-1</sup>) at 25 °C suggests that complex is non-electrolytic in nature. All the metal complexes have high melting points (>300 °C), except for the Cu<sup>2+</sup> (binary) complex, which is 214 °C. Elemental analyses and some physical properties of the isolated solid complexes are listed in Table 1.

### 4.1. IR spectra

The IR bands of 4-ethyl-1-(2-hydroxybenzoyl) thiosemicarbazide and its metal complexes are depicted in Table 2. The IR spectrum of **L**<sup>1</sup> in KBr shows a strong band at 1660 cm<sup>-1</sup> assignable to the ν(C=O) vibration [24,25]. This suggests that **L**<sup>1</sup> is mainly exists in the keto form. On the other hand, three bands are observed at 3126, 3186 and 3254 cm<sup>-1</sup> assigned to the ν(<sup>1</sup>NH), ν(<sup>2</sup>NH) and ν(<sup>4</sup>NH) vibrations [26], respectively. The three bands at 3388, 1244 and 700 cm<sup>-1</sup> are attributed to ν(OH) [25,26] and ν(C=S) [27] vibrations, respectively. Moreover, no bands are observed in the 2500–2600 cm<sup>-1</sup> region attributed to the SH group [28] indicating that the free ligand in the solid state is mainly existed in the thione/keto form (Fig. 1). The previous postulation is confirmed by molecular modeling of **L**<sup>1</sup> as shown in (Figs. 1a and 1b).

The IR spectra of metal complexes (binary complexes) show that **L**<sup>1</sup> acts as a mononegative bidentate in the thiol form in the case of binary Cu<sup>2+</sup> and Co<sup>2+</sup> chlorides complexes, while the ligand acts as a mononegative tetradentate in the enol form in case of the binary Zn<sup>2+</sup> acetate complex.

Firstly, in case of Cu<sup>2+</sup> and Co<sup>2+</sup> chloride complexes (Figs. 2 and 3), the results show that **L**<sup>1</sup> coordinates to the metal ions through

**Table 1**  
Analytical and some physical data of **L**<sup>1</sup> and its metal complexes.

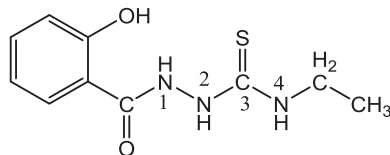
No.	Compound (empirical formula)	(F.Wt)	Color	M.p. (°C)	% Found (Calcd.)				$\mu_{\text{eff}}$ BM	$\Lambda_m^+$ (DMSO)
					C	H	M	Cl		
1	( <b>L</b> <sup>1</sup> ); C <sub>10</sub> H <sub>13</sub> N <sub>3</sub> O <sub>2</sub> S	239.3	White	217–218	50.6 (50.2)	5.3 (5.5)	–	–	–	
2	[Cu( <b>L</b> <sup>1</sup> -H) <sub>2</sub> ].EtOH	586.2	Brown	214	45.7 (45.1)	5.3 (5.2)	10.6 (10.8)	–	2.1	
3	[Co( <b>L</b> <sup>1</sup> -H) <sub>2</sub> ]	535.5	Black	>300	45.4 (44.9)	4.6 (4.6)	11.4 (11)	–	3.8	
4	[Zn <sub>2</sub> ( <b>L</b> <sup>1</sup> -H)(LH)(Ac) <sub>5</sub> ]	969.0	White	>300	38.1 (37.2)	4.4 (4.2)	21.1 (20.2)	–	–	
5	[Cu <sub>2</sub> ( <b>L</b> <sup>2</sup> ) <sub>2</sub> ( <b>L</b> <sup>1</sup> -2H) <sub>2</sub> (H <sub>2</sub> O) <sub>2</sub> ].4H <sub>2</sub> O	1022.0	Olive green	>300	46.6 (47)	4.3 (4.9)	12.2 (12.4)	–	1.7	
6	[Co( <b>L</b> <sup>2</sup> )( <b>L</b> <sup>1</sup> -2H)].3H <sub>2</sub> O	506.5	Deep brown	>300	46.9 (47.4)	4.5 (5)	11.4 (11.6)	–	4.2	
7	[Zn <sub>2</sub> ( <b>L</b> <sup>2</sup> )(OH)( <b>L</b> <sup>1</sup> -3H)(H <sub>2</sub> O)].1/2EtOH	581.3	White	>300	42.9 (43.4)	4.2 (4.2)	22.4 (22.6)	–	–	

<sup>+</sup>(ohm<sup>-1</sup> cm<sup>2</sup> mol<sup>-1</sup>), **L**<sup>2</sup> = 2,2'-dipyridyl.

**Table 2**  
IR spectral bands of **L**<sup>1</sup> and its metal complexes.

No.	Compound (empirical formula)	(F.Wt)	Color	M.p. (°C)	% Found (Calcd.)				$\mu_{\text{eff}}$ BM	$\lambda_{\text{m}}^+$ (DMSO)
					C	H	M	Cl		
1	(L; EHBTs)	239.301	White	217–218	50.6 (50.2)	5.3 (5.5)	–	–	–	–
2	[Cu(L-H) <sub>2</sub> ]-EtOH	586.195	Brown	214	45.7 (45.1)	5.3 (5.2)	10.6 (10.8)	–	2.1	10.8
3	[Co(L-H) <sub>2</sub> ]	535.516	Black	>300	45.4 (44.9)	4.6 (4.6)	11.4 (11)	–	3.8	15.2
4	[Zn <sub>3</sub> (L-H)(LH)(Ac) <sub>5</sub> ]	968.964	White	>300	38.1 (37.2)	4.4 (4.2)	21.1 (20.2)	–	–	–
5	[Cu <sub>2</sub> (dipy) <sub>2</sub> (L-2H) <sub>2</sub> (H <sub>2</sub> O) <sub>2</sub> ]-4H <sub>2</sub> O	1022.132	Olive green	>300	46.6 (47)	4.3 (4.9)	12.2 (12.4)	–	1.7	–
6	[Co(dipy)(L-2H)]-3H <sub>2</sub> O	506.453	Deep brown	>300	46.9 (47.4)	4.5 (5)	11.4 (11.6)	–	4.2	14.5
7	[Zn <sub>2</sub> (dipy)(OH)(L-3H)(H <sub>2</sub> O)]-(EtOH) <sub>1/2</sub>	581.289	White	>300	42.9 (43.4)	4.2 (4.2)	22.4 (22.6)	–	–	5.00

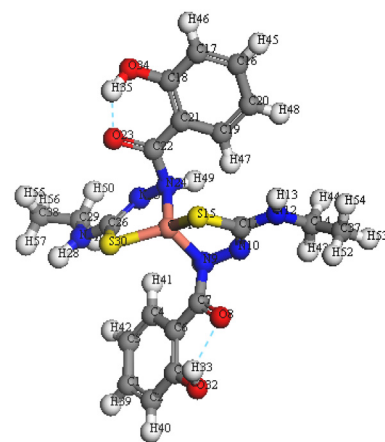
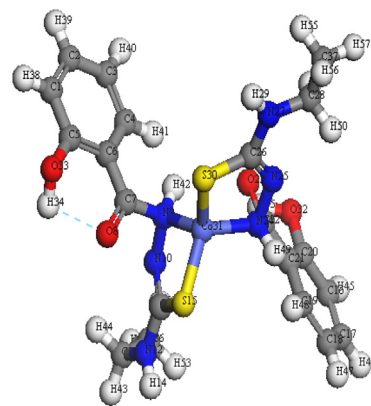
( $\text{ohm}^{-1} \text{cm}^2 \text{mol}^{-1}$ ), (dipy) = 2,2'-dipyridyl.

**Fig. 1.** Structure of **L**<sup>1</sup>.

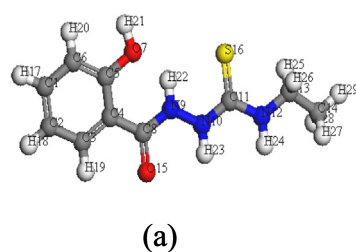
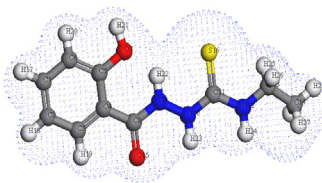
the C–SH with displacement of a hydrogen atom and the (<sup>1</sup>NH) group forming five-member ring around the metal ions. The formula of the Cu<sup>2+</sup> and Co<sup>2+</sup> chloride complexes is quite similar but differ only in the presence of one ethanol molecule outside the coordination sphere in case of Cu<sup>2+</sup> complex. The following evidences support the modes of chelation for the Cu<sup>2+</sup> and Co<sup>2+</sup> complexes

- (1) The disappearance of the CS band together with the appearance of a new band in the 1554–1557  $\text{cm}^{-1}$  region assigned to the (C=N\*) group which is taken as evidence for the enolization of the CS group together with the displacement of a hydrogen atom.
- (2) The shift of the band assigned to <sup>1</sup>NH as shown in Table 2 is taken as an evidence of participation of <sup>1</sup>NH group in bonding [25].
- (3) The results (Table 2) show the obscure of the band assigned to the (<sup>2</sup>NH) group due to the formation of the (C=N\*) group.
- (4) The observation of two new weak bands in the ranges 455–468 and 421–445  $\text{cm}^{-1}$  assigned to M–S and M–N vibrations [25,29], respectively, is taken as additional evidence for the participation of the <sup>1</sup>NH and the CS groups in bonding.
- (5) Also, the IR spectra show that the band assigned to  $\nu(\text{OH})$  (phenolic) in **L**<sup>1</sup> is shifted to lower wave-number and observed at 3353 and 3350  $\text{cm}^{-1}$  in the Cu<sup>2+</sup> and Co<sup>2+</sup> complexes, due to the formation of hydrogen bond [25].

On the other hand, in case of the Zn<sup>2+</sup> acetate complex (Fig. 4), the data show that two molecules of **L**<sup>1</sup> are coordinated to three

**Fig. 2.** Molecular modeling of [Cu(L<sup>1</sup>-H)<sub>2</sub>]-EtOH.**Fig. 3.** Molecular modeling of [Co(L<sup>1</sup>-H)<sub>2</sub>].

Zn<sup>2+</sup> ions. The first molecule of **L**<sup>1</sup> is coordinated to the first Zn(1) ion through the (CS) and (C=N\*) groups while it coordinates at the same time to the 2nd Zn(10) through the enolized carbonyl

**(a)****(b)****Figs. 1a and 1b.** Molecular modeling of **L**<sup>1</sup> (1a) and (1b) for electron density.

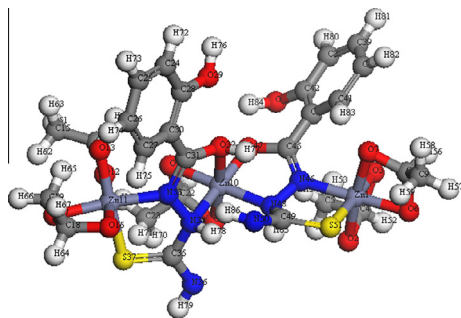


Fig. 4. Molecular modeling of  $[Zn_3(L^1-H)(LH)(Ac)_5]$ .

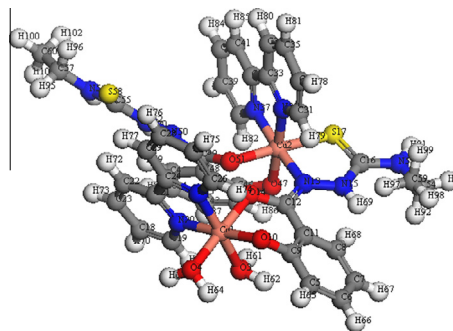


Fig. 5. Molecular modeling of  $[Cu_2(L^2)_2(L^1-2H)_2(H_2O)_2] \cdot 4H_2O$ .

oxygen ( $=C-OH$ ) with displacement of a hydrogen atom and the ( $^2NH$ ) groups forming five-membered ring around the  $Zn^{2+}$  ions. The second  $L^1$  is coordinating to the 3rd  $Zn(11)$  ion in a similar way to that observed for the first molecule of ligand coordinates to the 2nd  $Zn(10)$  ion through the  $^2NH$  and  $CO$  groups in the enol form without displacement of a hydrogen atom forming five-membered ring around the  $Zn^{2+}$  ion.

The following evidences support the mode of chelation in case of  $Zn^{2+}$  acetate:

- (1) The shift of the bands assigned to the (CS) group, which are observed in the  $(1235-1252)$  and  $(701-750\text{ cm}^{-1})$  ranges [25] as shown in Table 2. This indicates that the two CS groups from the two  $L^1$  are coordinated to the  $Zn^{2+}$  ions in the thio keto form without displacement of hydrogen atoms.
- (2) The disappearance of the band assigned to the ( $^1NH$ ) groups in the two  $L^1$  together with the appearance of new bands in the  $1567-1599\text{ cm}^{-1}$  range assigned to the azomethine groups ( $C=N^*$ ).
- (3) The shifts of the bands in the region  $3091-3094\text{ cm}^{-1}$  assigned to the ( $^2NH$ ) groups are taken as an evidence for the participation of the ( $^2NH$ ) groups in coordination.
- (4) The obscure of the band assigned to the (CO) group in case of first  $L^1$  molecule suggests that this group is coordinated to the 2nd  $Zn(10)$  ion in the enol form with displacement of a hydrogen atom, while the ligand coordinates in the enol form as in case of the 3rd  $Zn(11)$  ion without displacement of a hydrogen atom.
- (5) The IR spectrum of the  $Zn^{2+}$  acetate complex shows two bands at  $1518$  and  $1444\text{ cm}^{-1}$  assigned to  $\nu_{as}(Ac)$  and  $\nu_s(Ac)$  vibrations [25], respectively. The difference between these two bands is lower than  $176\text{ cm}^{-1}$  indicating the bidentate nature of the acetate group in bonding [30,31].

On comparing the IR spectra of the mixed  $Cu^{2+}$  complex with  $L^1$ , we observed the disappearance of the bands at  $3388$  and  $1660\text{ cm}^{-1}$  assigned to the (OH) and (CO) groups, respectively, which are existed  $L^1$  (Table 2). This indicates that these groups are participated in bonding by losing one proton from each group. The carbonyl oxygen group is enolized to form ( $=C-OH$ ) and consequently losses its proton together with the observation of new band at  $1351\text{ cm}^{-1}$  assigned to the (C–O). The CS group is shifted to lower wavenumber and observed at  $1238$  and  $686\text{ cm}^{-1}$  indicating that this group is coordinated to the 2nd  $Cu^{2+}$  ion without the formation of the  $-C-SH$  form [32]. Moreover, the IR spectrum shows the disappearance of the  $^1NH$  band together with the shifts of the  $^2NH$  to lower wavenumber ( $3108\text{ cm}^{-1}$ ) while the  $^4NH$  group is shifted to higher wavenumber ( $3257\text{ cm}^{-1}$ ) as shown in Table 2. The observation of two new bands in the spectrum of the  $Cu^{2+}$  mixed complex at  $1261$  and  $710\text{ cm}^{-1}$  assigned to the CS group [31] indicates that  $L^1$  molecule participates in bonding in the

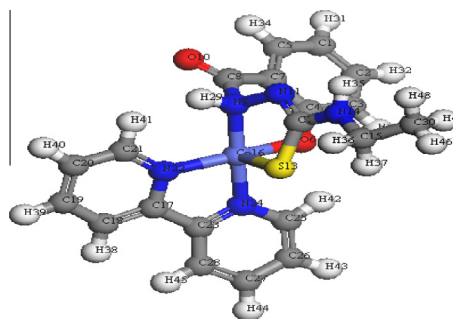


Fig. 6. Molecular modeling of  $[Co(L^2)(L^1-2H)] \cdot 3H_2O$ .

thio/keto form while the second  $L^1$  is excluded from bonding as shown in Fig. 5. Finally, the IR spectrum of the complex shows a broad medium band at  $3443\text{ cm}^{-1}$  assigned to water of coordination as well as the water of solvation. The new band observed at  $1110\text{ cm}^{-1}$  is assigned to  $\delta(OH)$  vibration [33] for the water of coordination. The bands observed at  $540$ ,  $490$ ,  $453$  and  $426\text{ cm}^{-1}$  are attributed  $\nu(M-O)$ ,  $\nu(M-S)$ ,  $\nu(M-N; \text{ligand})$  and  $(M-N; \text{dipy})$  vibrations [25,29], respectively. Also, the spectrum shows two bands at  $1525$  and  $1440\text{ cm}^{-1}$  assigned to the  $C=N$  groups of the 2,2'-dipyridyl ( $L^2$ ) which are obscured in the IR spectra of the binary complexes [25]. Another evidence for the participation of the OH (phenolic) in bonding in the  $Cu^{2+}$  complex comes from the negative test on adding  $FeCl_3$  solution [34].

The IR spectrum of the mixed ligand  $Co^{2+}$  complex (Fig. 6) shows bands at  $3283$ ,  $3151$ ,  $1666$ ,  $1553$ ,  $539$ ,  $495$ ,  $480$  and  $460\text{ cm}^{-1}$  assigned to  $\nu(^4NH)$ ,  $\nu(^1NH)$ ,  $\nu(C=O)$ ,  $\nu(C=N)$ ,  $\nu(M-O)$ ,  $\nu(M-S)$ ,  $\nu(M-N; \text{ligand})$  and  $\nu(M-N; 2,2'-\text{dipyridyl})$  vibrations [25,29], respectively. Also, the spectrum shows two bands at  $1540$  and  $1448\text{ cm}^{-1}$  assigned to the  $C=N$  groups of  $L^2$ , which are obscured in the IR spectra of the binary complexes [25].

The IR spectrum of the mixed  $Zn^{2+}$  complex (Fig. 7) shows two bands at  $1515$  and  $1444\text{ cm}^{-1}$  assigned to the  $C=N$  groups of 2,2'-dipyridyl which are obscured in the IR spectra of the binary complexes [25]. On comparing the IR spectra of the mixed  $Zn^{2+}$  complex with the free ligand, we observed the disappearance of the bands at  $3388$  and  $1660\text{ cm}^{-1}$  assigned to the (OH) phenolic and (CO) groups, existed in the free ligand, respectively (Table 2) indicating that these groups are participated in bonding by losing one proton from each group. The carbonyl oxygen group is enolized to form ( $=C-OH$ ) and consequently losses its proton. Another evidence for the participation of the OH (phenolic) in bonding in case of  $Zn^{2+}$  complex comes from the negative test on adding  $FeCl_3$  solution [34]. Also, we observed the disappearance of the bands at  $1244$  and  $700\text{ cm}^{-1}$  which are existed in  $L^1$  and assigned to the CS group due to the thioenolization but with displacement of a hydrogen atom indicating that this group is

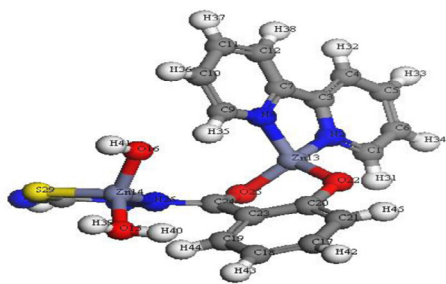


Fig. 7. Molecular modeling of  $[Zn_2(L^2)(OH)(L^1-3H)(H_2O)] \cdot 1/2EtOH$ .

participated in bonding. Moreover, the spectrum shows the disappearance of both the  $^1NH$  and  $^2NH$  bands while the  $^4NH$  band remains unaltered ( $3254\text{ cm}^{-1}$ ) as shown in Table 2. The observation of new bands at  $1599$  and  $1567\text{ cm}^{-1}$  assigned to the azomethine groups ( $C=N^*$ ) is taken as evidence for the displacement of two protons from the NH groups. The bands at  $540$ ,  $470$ ,  $456$  and  $446\text{ cm}^{-1}$  are attributed to the  $\nu(M-O)$ ,  $\nu(M-S)$ ,  $\nu(M-N; \text{ligand})$  and  $\nu(M-N; \text{dipy})$  vibrations [25,29], respectively. The band at  $1100\text{ cm}^{-1}$  is assigned to the hydroxyl ( $OH^-$ ) group [33], which is disappeared on deuteration. Finally, the spectrum of  $L^1$  shows a broad medium band at  $3448\text{ cm}^{-1}$  attributed to the water of coordination as well as the EtOH. The new band observed at  $1115\text{ cm}^{-1}$  is assigned to the  $\delta(OH)$  vibration of the coordinated water.

#### 4.2. $^1H$ NMR spectra

The  $^1H$ -NMR spectrum of  $L^1$  in  $d_6$ -DMSO shows several signals at  $11.9$ ,  $10.6$ ,  $9.4$  and  $8.1$  ppm, downfield with respect to TMS, which disappear upon adding  $D_2O$ . These signals are attributed to the protons of OH,  $^1NH$ ,  $^2NH$  and  $^4NH$ , respectively [35]. The multiple signals in the  $6.9$ – $7.9$  ppm range are corresponding to the aromatic phenyl protons. Also, the signals observed at  $3.44$  and  $1.07$  ppm are attributed to the protons of  $-CH_2$  and  $-CH_3$  groups [36], respectively. All these foundations suggest that  $L^1$  is mainly existed in the thione/keto form.

The  $^1H$ -NMR spectrum of  $[Zn_3(L^1-H)(LH)(Ac)_5]$  in  $d_6$ -DMSO shows the absence of the signal at  $10.6$  ppm, which is assigned to the ( $^1NH$ ) proton due to the formation of the azomethine group ( $C=N^*$ ). The signals appeared at  $1.1$ ,  $1.9$ ,  $3.4$  and  $4.3$  ppm are assigned to the protons of  $CH_3$  ( $C_2H_5^-$ ),  $CH_3$  ( $CH_3COO$ ),  $CH_3$  ( $CH_3COO$ ) attached to the 2nd Zn(II) ion and  $CH_2$  ( $C_2H_5^-$ ), respectively. The ( $^2NH$ ) signal undergoes a slight shift in its position ( $9.3$  ppm) due to its involvement in bonding. The ( $^4NH$ ) signal at  $8.1$  ppm remains without any shift suggesting that this group is not taking part in bonding. The  $^1H$ -NMR spectrum shows also

signals in the region  $6.8$ – $7.8$  ppm range assigned to the  $C_6H_4$ - protons. Also, the two signals observed at  $11.8$  and  $10.8$  ppm are assigned to the protons of OH (free, phenolic) and the enolized carbonyl oxygen ( $=C-OH$ ), respectively [37].

The  $^1H$ -NMR spectrum of  $[Zn_2(L^2)(OH)(L^1-3H)(H_2O)] \cdot 1/2EtOH$  in  $d_6$ -DMSO shows the disappearance of both the  $^1NH$  and  $^2NH$  signals while the  $^4NH$  signal remains existing at  $8.1$  ppm. This suggests the replacement of these two protons through enolization of both the CO and CS groups. The signals at  $9.4$ ,  $8.1$  and  $4.3$  ppm are assigned to the protons of OH (free)  $^4NH$  and OH ( $H_2O$ ), respectively. Also, the signals at  $1.05$ ,  $1.3$ ,  $3.4$ ,  $3.7$ ,  $6.9$ – $7.9$  and  $11.9$  are assigned to the protons of  $CH_3$  (ethyl),  $CH_3$  (EtOH),  $CH_2$  (ethyl),  $CH_2$  (EtOH), ph + dipy and OH (EtOH) [35,37], respectively.

#### 4.3. Mass spectra

The mass spectrum of  $L^1$  (Fig. 8) shows that the molecular ion peak is 239. This suggests that the structure of  $L^1$  has the chemical formula;  $C_{10}H_{13}N_3O_2S$  and M. Wt. =  $239.301$ . Also, the results of elemental analyses and  $^1H$ -NMR are taken as evidences for the proposed structure.

The fragmentation pattern of  $L^1$  shows corresponds to the successive degradation of the ligand ( $C_{10}H_{13}N_3O_2S$ ). The first peak at  $m/z$  239 represents the molecular ion (Calcd.  $239.301$ ). The peak in 152 correspond to  $[C_7H_7N_2O_2]^+$  (Calcd.  $151.43$ ) and the peak in 137 with represent of  $[C_7H_6NO_2]^+$  (Calcd.  $136.41$ ) fragment. There are signals which represent stepwise loss of NH, CO and OH fragments;  $[C_6H_5O_2]^+$  in 121 (Calcd.  $121.39$ ),  $[C_6H_5O]^+$  in 93 (Calcd.  $93.38$ ) and  $[C_6H_4]^+$  in 76 (Calcd.  $76.37$ ), respectively. The peak at 65 correspond to  $[C_5H_4]^+$  (Calcd.  $64.4$ ). The mass spectrum of  $[Co(L-H)_2]$  shows that the molecular ion peak is 535 (Fig. 9) while the theoretical value is  $535.516$ . Also, the elemental analyses are taken as evidences for the proposed structure.

The fragmentation pattern of this complex is shown in Scheme 1.

The mass spectrum of  $[Zn_2(L^2)(OH)(L^1-3H)(H_2O)] \cdot 1/2EtOH$  (Fig. 7) shows that the molecular ion peak  $[M]^+$  equals 580 is coincide with the theoretical value ( $581.289$ ) which can be taken as evidence for the presence of two  $Zn^{2+}$  ions coordinated to the donor atoms of  $L^1$  and  $L^2$  (Fig. 10).

The fragmentation pattern is represented by Scheme 2.

#### 4.4. Electronic spectra and magnetic behavior

The electronic spectrum of  $L^1$  in Nujol mull shows three bands at  $37,879$ ,  $32,051$  and  $29,762\text{ cm}^{-1}$  assigned to  $\pi \rightarrow \pi^*$  (CO),  $n \rightarrow \pi^*$  (CO) and  $n \rightarrow \pi^*$  (CS), respectively. The data suggest that  $L^1$  is mainly existed in the keto form [38]. The electronic spectrum of

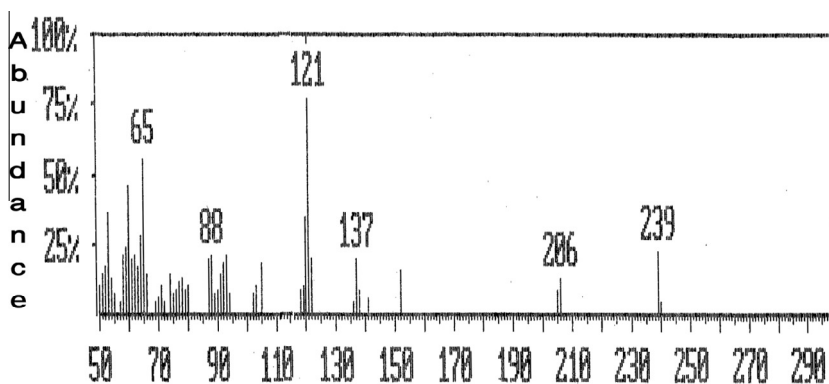


Fig. 8. Mass spectrum of  $L^1$ .

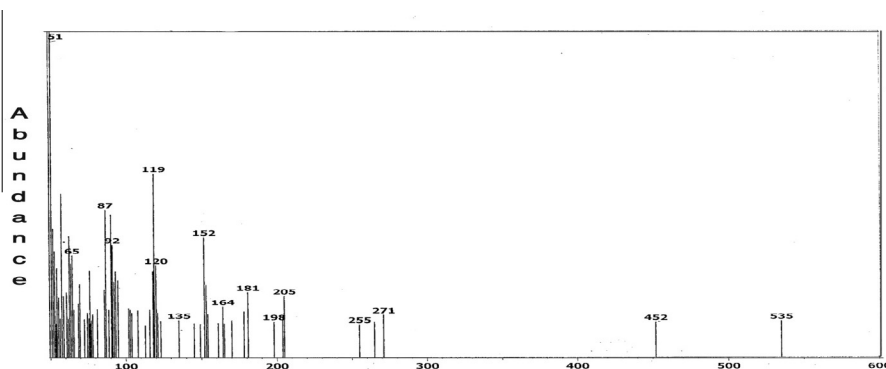
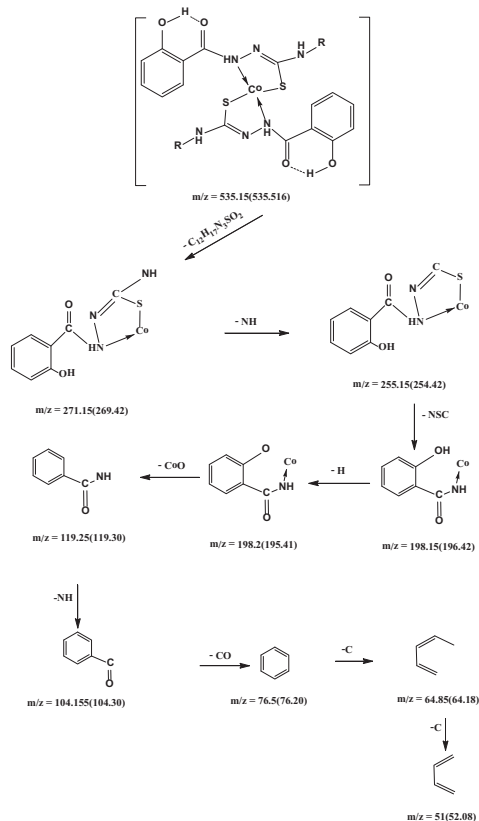


Fig. 9. Mass spectrum of  $[\text{Co}(\text{L}^1\text{-H})_2]$ .



Scheme 1. Fragmentation pattern of  $[\text{Co}(\text{L}^1\text{-H})_2]$ .

the  $\text{Cu}^{2+}$  binary complex in Nujol shows two bands at 14,390 and 17,825  $\text{cm}^{-1}$  assigned to the  ${}^2\text{B}_2 \rightarrow {}^2\text{E}$  and  ${}^2\text{B}_2 \rightarrow {}^2\text{B}_1$  transitions in a tetrahedral geometry around the  $\text{Cu}^{2+}$  ion [39]. Also, the bands at 19,360 and 20,580  $\text{cm}^{-1}$  are assigned to charge-transfer of the type (L  $\rightarrow$  M) transition. Moreover, the value of the corrected magnetic moment ( $\mu_{\text{eff}} = 2.1$  BM) suggests the absence of any Cu–Cu interaction [40].

The electronic spectrum of the  $\text{Co}^{2+}$  binary complex shows four bands at 14,990, 17,125, 18,940 and 21,277  $\text{cm}^{-1}$ . The first band is attributed to  ${}^4\text{A}_2 \rightarrow {}^4\text{T}_1$  (F) in a tetrahedral geometry around the  $\text{Co}^{2+}$  ion. The second band at 17,125  $\text{cm}^{-1}$  is assigned to  ${}^4\text{A}_2 \rightarrow {}^4\text{T}_1$  (P) [41]. The other two bands at 18,940 and 21,277  $\text{cm}^{-1}$  are assigned to charge-transfer (L  $\rightarrow$  M). Also, the value of the corrected magnetic moment ( $\mu_{\text{eff}} = 3.8$  BM) is taken as a strong evidence for the existence of a tetrahedral geometry around the  $\text{Co}^{2+}$  ion [42]. The electronic spectrum of the mixed ligand  $\text{Cu}^{2+}$  complex shows bands at 13,910, 14,535, 16,920,

18,520, 21,100 and 22,940  $\text{cm}^{-1}$ . The first and the third bands are assigned to the  ${}^2\text{E}_g \rightarrow {}^2\text{T}_{2g}$  transition in a distorted-tetragonal geometry containing  $\text{N}_2\text{O}_4$  donor atoms around the  ${}^1\text{Cu}^{2+}$  while the second and fourth bands are attributed to the  ${}^2\text{E}_g \rightarrow {}^2\text{T}_{2g}$  transition in a distorted-tetragonal geometry around the second  $\text{Cu}^{2+}$  but containing  $\text{N}_3\text{O}_2\text{S}$  donor atoms [39]. Also the two bands at 21,100 and 22,940  $\text{cm}^{-1}$  are assigned to charge-transfer (L  $\rightarrow$  M). The average magnetic moment ( $\mu_{\text{eff}} = 1.7$  BM) suggests the absence of Cu–Cu interaction [40].

The electronic spectrum of the  $\text{Co}^{2+}$  complex,  $[\text{Co}(\text{L}^2)(\text{L-2H})] \cdot 3\text{H}_2\text{O}$ , in Nujol shows three bands at 16,610, 18,660 and 21,190  $\text{cm}^{-1}$ . The first two bands are assigned to  ${}^4\text{A}_2 \rightarrow {}^4\text{A}_1$  and  ${}^4\text{A}_2 \rightarrow {}^4\text{E}$  transitions in a high-spin square pyramidal around the  $\text{Co}^{2+}$  ion [39]. The band observed at 21,190  $\text{cm}^{-1}$  is assigned to charge-transfer (L  $\rightarrow$  M). Also, the corrected magnetic moment value ( $\mu_{\text{eff}} = 4.2$  BM) is taken as additional evidence for the proposed structure [40].

#### 4.5. Molecular modeling

##### 4.5.1. Geometry optimization with DFT method

The optimized molecular structures of  $\text{L}^1$  and its metal complexes are shown in Figs. 1–7. For the discussion of optimized molecular geometry bond lengths and angles are calculated and given in Tables (S1–S14). The following remarks can be concluded:

- (1) The bond angles of the  $\text{L}^1$  are altered somewhat upon coordination; the largest change affects C(4)–C(5)–O(7), C(4)–C(8)–O(15), N(9)–C(8)–O(15) and S(16)–C(11)–N(10), which are reduced or increased on complex formation as a consequence of bonding [43].
- (2) The bond angles in case of  $[\text{Cu}(\text{L}^1\text{-H})_2] \cdot \text{EtOH}$ ,  $[\text{Co}(\text{L}^1\text{-H})_2]$  binary and  $[\text{Zn}_2(\text{L}^2)(\text{OH})(\text{L}^1\text{-3H})(\text{H}_2\text{O})] \cdot 1/2\text{EtOH}$  ternary complexes afforded a tetrahedral geometry, while in the  $[\text{Zn}_3(\text{L}^1\text{-H})(\text{LH})(\text{Ac})_5]$  binary and  $[\text{Cu}_2(\text{L}^2)_2(\text{L}^1\text{-2H})_2(\text{H}_2\text{O})_2] \cdot 4\text{H}_2\text{O}$  ternary are quite near to an octahedral geometry predicting, and adopts a square-pyramidal arrangement in  $[\text{Co}(\text{L}^2)(\text{L}^1\text{-2H})] \cdot 3\text{H}_2\text{O}$  ternary.
- (3) All the active groups taking part in coordination have bond lengths longer than that already exist in the ligand (like C–S and CO) [43].
- (4) The bond angles within the  $\text{L}^1$  backbone do not change significantly but the angles around the metal undergo appreciable variations upon changing the metal center.

#### 4.6. Chemical reactivity

##### 4.6.1. Global reactivity descriptors

The determination of energies of the HOMO ( $\pi$  donor) and LUMO ( $\pi$  acceptor) are important parameters in quantum chemical

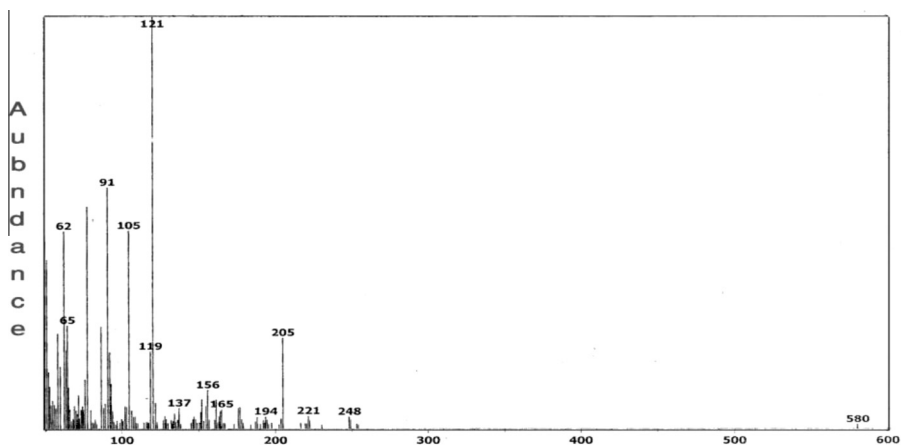
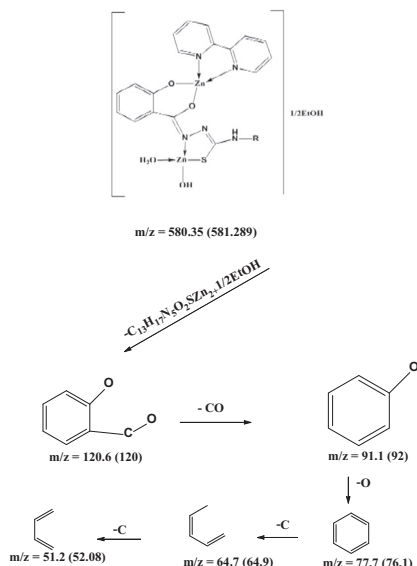


Fig. 10. Mass spectrum of  $[Zn_2(L^2)(OH)(L^1-3H)(H_2O)] \cdot 1/2EtOH$ .



Scheme 2. Fragmentation pattern of  $[Zn_2(L^2)(OH)(L^1-3H)(H_2O)] \cdot 1/2EtOH$ .

calculations. The HOMO (Highest Occupied Molecular Orbitals) is the orbital that primarily acts as an electron donor and the LUMO (Lowest Unoccupied Molecular Orbital) is the orbital that largely act as the electron acceptor. These molecular orbitals are also called the frontier molecular orbitals (FMOs).

- (i) The  $E_{HOMO}$  and  $E_{LUMO}$  and their neighboring orbitals are all negative, which indicate that the prepared complexes are stable [44].
- (ii) The FMO's theory predicts sites of coordination (electrophilic attack) on aromatic compounds. An initial assumption is that the reaction takes place with maximum overlap between the HOMO on one molecule and the LUMO on the other. The overlap between the HOMO and the LUMO is a governing factor in many reactions. We can indicate that from the calculation by searching for the largest values of molecular orbital coefficients. So, orbitals of the ligand with the largest value of molecular orbital coefficients may be considered as the sites of coordination. This conclusion is confirmed by the data obtained from the calculation because the oxygen of the C=O group, nitrogen of C–NH and sulfur C=S have the largest values of molecular orbital coefficients.

- (iii) Gutmann's variation rules, "the bond strength increases as the adjacent bonds become weakness" such as found by Linert et al. [45]. This interpretation agrees well with the resultant as the increase of the  $E_{HOMO}$  is accompanied by a weakness (elongation) of the metal–ligand bonds, which leads to a strengthening (shortness) of the sites adjacent to the metal ligand centers.
- (iv) The HOMO level is mostly localized on the O(15) N(9) and S(16) atoms (Fig. 11), indicating that these atoms are the preferred sites for nucleophilic attack at the central metal ion. This means that these moieties, with high coefficients of HOMO density, are oriented toward the metal ions.
- (v) The energy gap ( $E_{HOMO} - E_{LUMO}$ ) is an important stability index helps to characterize the chemical reactivity and kinetic stability of the molecule [46]. A molecule with a small gap is more polarized and is known as soft molecule. Soft molecules are more reactive than hard ones because they easily offer electrons to an acceptor. The energy gap is small in  $L^1$  indicating that charge-transfer easily occurs in

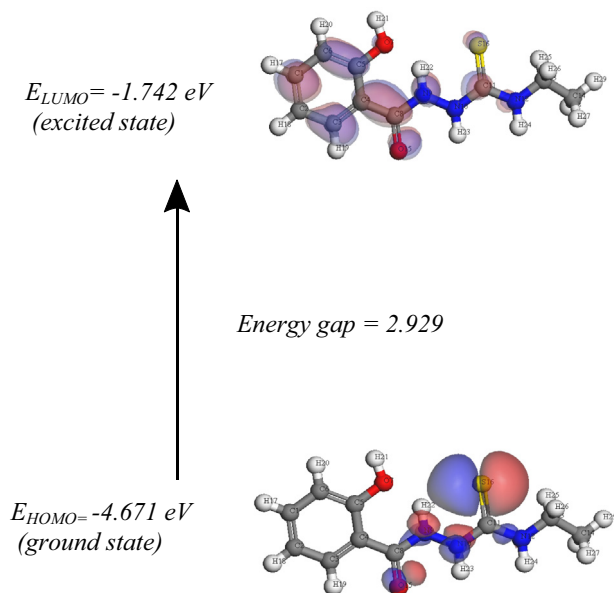
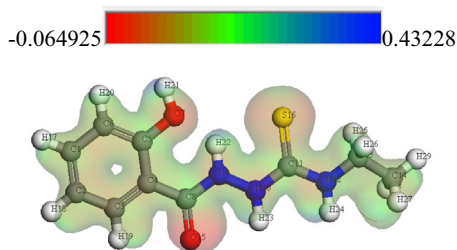


Fig. 11. 3D plots frontier orbital energies using DFT method for  $L^1$ .

**Table 3**  
Calculated  $E_{\text{HOMO}}$ ,  $E_{\text{LUMO}}$ , energy band gap ( $E_{\text{H}} - E_{\text{L}}$ ), chemical potential ( $\mu$ ), electronegativity ( $\chi$ ), global hardness ( $\eta$ ), global softness ( $S$ ) and global electrophilicity index ( $\omega$ ) for  $\text{L}^1$  and its complexes.

No.	Compound	$E_{\text{H}}$ (eV)	$E_{\text{L}}$ (eV)	$(E_{\text{H}} - E_{\text{L}})$ (eV)	$\chi$ (eV)	$\mu$ (eV)	$\eta$ (eV)	$S$ ( $\text{eV}^{-1}$ )	$\omega$ (eV)	$\sigma$ (eV)
1	( $\text{L}^1$ ): $\text{C}_{10}\text{H}_{13}\text{N}_3\text{O}_2\text{S}$	-4.671	-1.742	-2.929	3.2065	-3.2065	1.4645	0.73225	7.528733	0.682827
2	$[\text{Cu}(\text{L}^1\text{-H})_2] \cdot \text{EtOH}$	-4.823	-2.119	-2.704	3.471	-3.471	1.352	0.676	8.144341	0.739645
3	$[\text{Co}(\text{L}^1\text{-H})_2]$	-4.180	-2.764	-1.416	3.472	-3.472	0.708	0.354	4.267394	1.412429
4	$[\text{Zn}_3(\text{L}^1\text{-H})(\text{LH})(\text{Ac})_5]$	-5.276	-3.185	-2.091	4.2305	-4.2305	1.0455	0.52275	9.355725	0.95648
5	$[\text{Cu}_2(\text{L}^2)_2(\text{L}^1\text{-2H})_2(\text{H}_2\text{O})_2] \cdot 4\text{H}_2\text{O}$	-4.316	-2.233	-2.083	3.2745	-3.2745	1.0415	0.52075	5.583664	0.960154
6	$[\text{Co}(\text{L}^2)(\text{L}^1\text{-2H})] \cdot 3\text{H}_2\text{O}$	-3.706	-3.085	-0.621	3.3955	-3.3955	0.3105	0.15525	1.789942	3.220612
7	$[\text{Zn}_2(\text{L}^2)(\text{OH})(\text{L}^1\text{-3H})(\text{H}_2\text{O})] \cdot (\text{EtOH})_{1/2}$	-4.45	-3.445	-1.005	3.9475	-3.9475	0.5025	0.25125	3.915168	1.99005

H = HOMO, L = LUMO.



**Fig. 12.** Molecular electrostatic potential map for  $\text{L}^1$ .

it, which influences the biological activity of the molecule. Low value of energy gap is also due to the groups that enter into conjugation [47].

- (vi) The lower HOMO energy values show that molecules donating electron ability is the weaker. On contrary, the higher HOMO energy implies that the molecule is a good electron donor. LUMO energy presents the ability of a molecule-receiving electron [46].

DFT method's concept was used to calculate the chemical reactivity and site selectivity of the molecular systems. The energies of frontier molecular orbitals ( $E_{\text{HOMO}}$ ,  $E_{\text{LUMO}}$ ), energy band gap ( $E_{\text{HOMO}} - E_{\text{LUMO}}$ ) which explains the eventual charge-transfer interaction within the molecule, electronegativity ( $\chi$ ), chemical potential ( $\mu$ ), global hardness ( $\eta$ ), global softness ( $S$ ) and global electrophilicity index ( $\omega$ ) [48,49] are listed in Table 3.

$$\chi = -1/2 (E_{\text{LUMO}} + E_{\text{HOMO}}) \quad (1)$$

$$\mu = -\chi = 1/2 (E_{\text{LUMO}} + E_{\text{HOMO}}) \quad (2)$$

$$\eta = 1/2 (E_{\text{LUMO}} - E_{\text{HOMO}}) \quad (3)$$

$$S = 1/2 \eta \quad (4)$$

$$\omega = \mu^2/2 \eta \quad (5)$$

The inverse value of the global hardness is designed as the softness  $\sigma$  as follow:

$$\sigma = 1/\eta \quad (6)$$

Electrophilicity index is one of the most important quantum chemical descriptors in describing toxicity of various pollutants in terms of their reactivity and site selectivity [50]. Also the electrophilicity properly quantifies the biological activity of drug receptor interaction. This new reactivity index measures the stabilization in energy when the system acquires an additional electronic charge from the environment. The importance of  $\eta$  and  $\sigma$  is to measure the molecular stability and reactivity. In a complex

formation system,  $\text{L}^1$  acts as a Lewis base while the metal ion acts as a Lewis acid. Metal ions are hard acids and  $\text{L}^1$  is hard base, which facilitate the complex formation.

#### 4.7. Molecular electrostatic potential (MEP)

The MEP is a plot of electrostatic potential mapped onto the constant electron density surface. It is also very useful in research of molecular structure with its physicochemical property relationship as well as hydrogen bonding interactions [51–53]. The electrostatic potential  $V(r)$  at a given point  $r$  ( $x, y, z$ ) is defined in terms of the interaction energy between the electrical charge generated from the molecule electrons, nuclei and proton located at  $r$  [54,55]. In the present study, 3D plots of molecular electrostatic potential (MEP) of  $\text{L}^1$  (Fig. 12) have been drawn. The maximum negative region, which preferred site for electrophilic attack appears as a red color, the maximum positive region that preferred site for nucleophilic attack symptoms is observed as a blue color. Potential increases in the order red < green < blue, where blue shows the strongest attraction and red shows the strongest repulsion. Regions having the negative potential are over the electronegative atoms while the regions having the positive potential are over the hydrogen atoms.

#### 4.8. Other molecular properties

The calculations of the binding energy revealed that the increase of the value of the calculated binding energy of complexes compared to that of  $\text{L}^1$  indicating that the stability of the formed metal complexes are higher than that of  $\text{L}^1$ . Also, the energy components were calculated by DFT method as shown in Table 4.

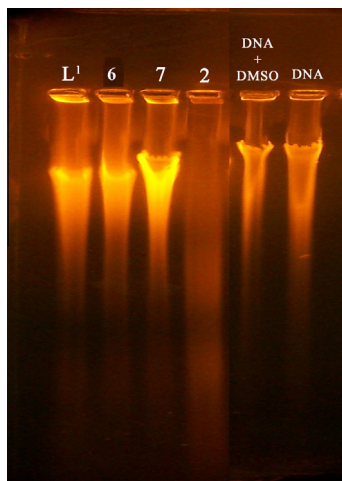
#### 4.9. Thermogravimetric studies

Thermal analysis plays an important role in shedding light on bonding in metal complexes. To make sure about the proposed formula and structure of the complexes under investigation, thermal analyses (TGA and DTG) curves of the complexes were carried out within a temperature range from 25 up to 800 °C. The estimated mass losses were computed based on the TGA results and the calculated mass losses are computed using the results of microanalyses (Table S15).

The TGA curve of the  $\text{Cu}^{2+}$  complex,  $[\text{Cu}(\text{L}^1\text{-H})_2] \cdot \text{EtOH}$ , shows that the complex decomposes in four steps as shown in Fig. S1. The first step lays in the temperature range 50–93 °C corresponding to the loss of EtOH molecule which existing outside the coordination sphere (Found: 8.4%; Calcd. 7.8%). The second step is observed at 234 °C attributed to the loss of  $\text{C}_{15}\text{H}_{11}\text{N}_2\text{O}_4$  (Found: 47.1%; Calcd. 46.3%). The third step is recorded at 340 °C attributed to the loss of  $\text{C}_2\text{H}_7\text{N}_2$  (Found: 11.2%; Calcd. 10.1%). The fourth step is observed in the temperature range 446–624 °C and attributed to the loss of  $\text{C}_3\text{H}_6\text{N}_2\text{S}$  (Found: 16.8%; Calcd. 17.4%). Finally, the estimated residue is corresponding to CuS (Found: 16.5%; Calcd. 16.3%).

**Table 4**Some of energetic properties of **L**<sup>1</sup> and its complexes calculated by DMOL<sup>3</sup> using DFT-method.

No.	Compound	HOMO (eV)	LOMO (eV)	Binding energy (kcal/mol)	Total energy (kcal/mol)	Dipole moment (D)
1	( <b>L</b> <sup>1</sup> ); C <sub>10</sub> H <sub>13</sub> N <sub>3</sub> O <sub>2</sub> S	-4.671	-1.742	-3066.9	-6.9 × 10 <sup>5</sup>	0.7909
2	[Cu( <b>L</b> <sup>1</sup> -H) <sub>2</sub> ]-EtOH	-4.823	-2.119	-6084.4	-1.5 × 10 <sup>6</sup>	3.6168
3	[Co( <b>L</b> <sup>1</sup> -H) <sub>2</sub> ]	-4.180	-2.764	-6163.9	-1.4 × 10 <sup>6</sup>	1.5945
4	[Zn <sub>3</sub> ( <b>L</b> <sup>1</sup> -H)(LH)(Ac) <sub>5</sub> ]	-5.276	-3.185	-9382.7	-2.4 × 10 <sup>6</sup>	6.3131
5	[Cu <sub>2</sub> ( <b>L</b> <sup>2</sup> ) <sub>2</sub> ( <b>L</b> <sup>1</sup> -2H) <sub>2</sub> (H <sub>2</sub> O) <sub>2</sub> ]-4H <sub>2</sub> O	-4.316	-2.233	-11895.6	-2.3 × 10 <sup>6</sup>	1.1607
6	[Co( <b>L</b> <sup>2</sup> )( <b>L</b> <sup>1</sup> -2H)]-3H <sub>2</sub> O	-3.706	-3.085	-5486.2	-1.1 × 10 <sup>6</sup>	7.8554
7	[Zn <sub>2</sub> ( <b>L</b> <sup>2</sup> )(OH)( <b>L</b> <sup>1</sup> -3H)(H <sub>2</sub> O)]-1/2EtOH	-4.45	-3.445	-5080.2	-1.3 × 10 <sup>6</sup>	9.9962

**Fig. 13.** Biological effect of **L**<sup>1</sup> and its Cu<sup>2+</sup> (**2**), Co<sup>2+</sup> (**6**) and Zn<sup>2+</sup> (**7**) complexes.

The TGA curve of [Zn<sub>3</sub>(**L**<sup>1</sup>-H)(LH)(Ac)<sub>5</sub>] shows that the complex decomposes in three steps (Fig. S2). The first step lies at 382 °C corresponding to the loss of C<sub>3</sub>H<sub>4</sub>O<sub>3</sub> (Found: 8.6%; Calcd. 9.1%). The second step is observed at 475 °C attributed to the loss of C<sub>14</sub>H<sub>16</sub>O<sub>9</sub> (Found: 32.4%; Calcd. 33.8%). The third step is observed at 533 °C attributed to the loss of C<sub>9</sub>H<sub>11</sub>NO<sub>2</sub> (Found: 17.6%; Calcd. 17%). Finally, the estimated residue corresponds to Zn<sub>3</sub> + C<sub>4</sub>H<sub>9</sub>N<sub>5</sub>S<sub>2</sub> (Found: 40.4%; Calcd. 40%).

The amount of water in the Cu<sup>2+</sup> ternary complex, [Cu<sub>2</sub>(**L**<sup>2</sup>)(**L**<sup>1</sup>-2H)<sub>2</sub>(H<sub>2</sub>O)]-4H<sub>2</sub>O, was determined gravimetrically at 120 °C. The results show that the complex losses 4H<sub>2</sub>O (Found: 7.1%; Calcd. 6.7%) at 120 °C. This suggests the loss of the water outside the coordination sphere.

The TGA curve of the Co<sup>2+</sup> ternary complex, [Co(**L**<sup>2</sup>)(**L**<sup>1</sup>-2H)]-3H<sub>2</sub>O, shows that the complex decomposes in five steps as shown in Fig. S3. The first step lies at 60.9 °C corresponds to the loss of H<sub>2</sub>O molecules outside the coordination sphere (Found: 3.5%; Calcd. 3.6%). The second step is observed in the temperature range 123–275 °C attributed to the loss of C<sub>3</sub>H<sub>6</sub>N + 2H<sub>2</sub>O (Found: 17.6%; Calcd. 18.2%). The third step is observed in the temperature range 364–450 °C attributed to the loss of C<sub>10</sub>H<sub>8</sub>N<sub>2</sub> (Found: 32.7%; Calcd. 30.8%). The fourth step is observed at 551 °C attributed to the loss of C<sub>6</sub>H<sub>4</sub> (Found: 15.3%; Calcd. 15%). Step five is observed at 661 °C attributed to the loss of CHN<sub>2</sub>O (Found: 11.3%; Calcd. 10.5%). Finally, the estimated residue is to CoOS (Found: 19.6%; Calcd. 20.9%).

The amount of solvents in [Zn<sub>2</sub>(**L**<sup>2</sup>)(OH)(**L**<sup>1</sup>-3H)(H<sub>2</sub>O)]-1/2EtOH was determined gravimetrically at 120 °C. The results show the loss of 1/2EtOH at 120 °C which is existed outside the coordination sphere (Found 3.96%; Calcd. 4.15%).

#### 4.10. DNA studies

The results show that **L**<sup>1</sup> and its metal complexes have low effects on the Calf-Thymus (DNA) as shown in Fig. 13. The results

suggest that the binary complexes are more effective than the ternary complexes for the Calf-Thymus and can be arranged in the following order:

[Cu(**L**<sup>1</sup>-H)<sub>2</sub>]-EtOH (**2**) (sp<sup>3</sup>) > [Zn<sub>2</sub>(**L**<sup>2</sup>)(OH)(**L**<sup>1</sup>-3H)(H<sub>2</sub>O)]-1/2EtOH (**7**) (sp<sup>3</sup>) > [Co(**L**<sup>2</sup>)(**L**<sup>1</sup>-2H)]-3H<sub>2</sub>O (**6**) (dsp<sup>3</sup>) > (**L**<sup>1</sup>), in comparison to the control sample.

## 5. Conclusion

Different types of binary and ternary metal complexes derived from 4-ethyl-1-(2-hydroxybenzoyl) thiosemicarbazide and 2,2'-dipyridyl have been synthesized and characterized. These complexes are quite similar to these separated from 4-allyl- and 4-phenyl-1-(2-hydroxybenzoyl) thiosemicarbazides. Uncommon geometries of Co<sup>2+</sup> and Zn<sup>2+</sup> have been characterized on the basis of the spectral and magnetic data. Also, the hydroxo-complex with the general formula, [Cu<sub>2</sub>(**L**<sup>2</sup>)(**L**<sup>1</sup>-2H)(OH)<sub>2</sub>H<sub>2</sub>O], was synthesized by adjusting the pH of the solution using KOH solution. A comparison of the ligands derived from ethyl, allyl and phenyl on the Calf-Thymus (DNA) can conclude the following remarks:

The results suggest that the ethyl group is more effective since this group is electron-donating group, which increases the electron density on the thioketo group and hence increases its effect on the interaction with both the metal salts and Calf-Thymus (DNA). Also, the presence of this small group is easily penetrated inside the chain of the Calf-Thymus (DNA) and consequently it will be more effective. In case of phenyl the effect is small than the ethyl, this may be due to size of phenyl ring. In case of allyl ligand the existence of withdrawal group (allyl group) decreases the electron density on the thioketo group (C=S) and hence it has no effects on the DNA. In comparing the dipole moment and energy band gap for the three ligands, the data show that the ligand containing ethyl group is smaller than other two ligands (phenyl and allyl).

## Appendix A. Supplementary data

Supplementary data associated with this article can be found, in the online version, at <http://dx.doi.org/10.1016/j.saa.2015.06.056>.

## References

- [1] K.J. Duffy, A.N. Shaw, E. Delorme, S.B. Dillon, C. Erickson-Miller, L. Giampa, Y. Huang, R.M. Keenan, P. Lamb, N. Liu, S.G. Miller, A.T. Price, J. Rosen, H. Smith, K.J. Wiggall, L. Zhang, J.I. Luengo, J. Med. Chem. 45 (2002) 3573–3575.
- [2] X. Du, C. Guo, E. Hansel, P.S. Doyle, C.R. Caffrey, T.P. Holler, J.H. McKerrow, F.E. Cohen, J. Med. Chem. 45 (2002) 2695–2707.
- [3] D. Kovala-Demertzi, M.A. Demertzi, E. Filiou, A.A. Pantazaki, P.N. Yadav, J.R. Miller, Y. Zheng, D.A. Kyriakidis, Biomaterials 16 (2003) 411–418.
- [4] J.P. Scovill, D.L. Klayman, C.F. Franchino, J. Med. Chem. 25 (1982) 1261–1264.
- [5] A. Papageorgiou, Z. Iakovidou, D. Mourelatos, E. Mioglou, L. Boutis, A. Kotsis, D. Kovala-Demertzi, A. Domopoulou, D.X. West, M.A. Demertzi, Anticancer Res. 17 (1997) 247–251.
- [6] D.L. Klayman, J.P. Scovill, J.F. Bartosevich, C.J. Mason, J. Med. Chem. 22 (1979) 1367–1373.
- [7] C. Shipman Jr., S.H. Smith, J.C. Drach, D.L. Klayman, Antiviral Res. 6 (1986) 197–222.
- [8] M.M. Mostafa, D.X. West, Trans. Met. Chem. 8 (1983) 304–308.
- [9] M.M. Mostafa, D.X. West, Trans. Met. Chem. 8 (1983) 312–315.

- [10] A.A. El-Asmy, M.M. Bekheit, M.M. Mostafa, *Synth. React. Inorg. Met.-Org. Chem.* 15 (1985) 1247–1259.
- [11] A.A. El-Asmy, M.M. Bekheit, K.M. Ibrahim, M.M. Mostafa, *Acta Chim. Acad. Sci. (Hung)* 121 (1986) 386–391.
- [12] M.E. Khalifa, A.A. El-Asmy, K.M. Ibrahim, M.M. Mostafa, *Synth. React. Inorg. Met.-Org. Chem.* 16 (1986) 1305–1317.
- [13] A.A. El-Asmy, M.M. Bekheit, K.M. Ibrahim, M.M. Mostafa, *Synth. React. Inorg. Met.-Org. Chem.* 16 (1986) 1453–1462.
- [14] Y. Harek, A.K.T. Maki, M.M. Mostafa, *Spectrochim. Acta* 48A (1992) 1191–1194.
- [15] A.A. El-Asmy, T.Y. Al-Ansi, R.R. Amine, *Polyhedron* 9 (1990) 2029–2034.
- [16] M.E. Khalifa, T.H. Rakha, M.M. Bekhiet, *Synth. React. Inorg. Met.-Org. Chem.* 26 (1996) 1149–1161.
- [17] A.A. Abo-Hussen, S.S. Elkholy, M.Z. Elsabee, *J. Coord. Chem.* 57 (2004) 1027–1036.
- [18] I.T. Ahmed, *Trans. Met. Chem.* 32 (2007) 674–682.
- [19] S.S. Kandil, Phosphorous, Sulfur, Silicon, *Relat. Elem.* 185 (2010) 2455–2463.
- [20] M.R. Mlahi, S.G. Azhari, M.M. Mostafa, *Spectrochim. Acta* 134 (2015) 465–472.
- [21] S.J. Azhari, M.R. Mlahi, A.A. El-Asmy, M.M. Mostafa, *Spectrochim. Acta* 134 (2014) 465–472.
- [22] A.I. Vogel, *A Text Book of Quantitative Inorganic Chemistry*, Longmans, London, 1961.
- [23] G.A. Bain, F. John, *J. Chem. Educ.* 85 (2008) 532–536.
- [24] S.Y. Chundak, V.M. Leovac, D.Z. Obadovic, D.M. Petrovic, *Trans. Met. Chem.* 11 (1986) 308–312.
- [25] K. Nakamoto, *Infrared Spectra of Inorganic and Coordination Compounds*, John Wiley, New York, 1970.
- [26] S.I. Mostafa, M.M. Bekheit, M.M. El-Agez, *Synth. React. Inorg. Met.-Org. Chem.* 30 (2000) 2029–2049.
- [27] M.M. Bekheit, *Synth. React. Inorg. Met.-Org. Chem.* 20 (1990) 1273–1284.
- [28] M.P. Peotia, J.N. Gurtu, V.B. Rana, *Ind. J. Chem.* 19A (1980) 133.
- [29] J.R. Ferraro, *Low Frequency Vibrations of Inorganic and Coordination Compounds*, Plenum Press, New York, 1966.
- [30] A. Szorcisk, L. Nagy, L. Pellerito, T. Yamaguchi, K. Yoshida, *J. Radioanal. Nucl. Chem.* 256 (2003) 3–10.
- [31] J.P. Josiniki, J.R. Bianchani, J. Cueve, F.A. El-Saied, A.A. El-Asmy, D.X. West, *Z. Allg. Chem.* 629 (2003) 202–206.
- [32] L.J. Bellamy, *The Infrared Spectra of Complex Molecules*, Methuen, London, 1966.
- [33] J.R. Ferraro, W.R. Walker, *Inorg. Chem.* 4 (10) (1965) 1382–1386.
- [34] F. Feigl, *Spot Tests in Inorganic Analysis*, Elsevier, Amsterdam, 1966.
- [35] K.C. Rageovic, V.V. Kakurinov, D.G. Molnar, A. Buzarovska, *Molecules* 6 (2001) 815–824.
- [36] M.M. Mostafa, *Spectrochim. Acta* 66A (2007) 480–486.
- [37] R.M. Silverstein, G.C. Bassler, *Spectroscopic Identification of Organic Compounds*, Wiley, New York, 1967.
- [38] C.N.R. Rao, *Ultraviolet and Visible Spectroscopy*, Plenum Press, New York, 1975.
- [39] A.B.P. Lever, *Inorganic Electronic Spectroscopy*, Elsevier, Amsterdam, 1968.
- [40] M. Kato, K.B. Jonassen, G.C. Fanning, *Chem. Rev.* 64 (1964) 99128.
- [41] S.F.A. Kettle, *Coordination Compounds*, Thomas Nelson and Sons Ltd, London, 1969.
- [42] J. Lewis, R.G. Wilkins, *Modern Coordination Chemistry*, Interscience, New York, 1960.
- [43] D.X. West, J.K. Swearingen, J. Valdés-Martinez, S. Hernández-Ortega, A.K. El-Sawaf, F.V. Meurs, A. Castiñeiras, I. Garcia, E. Bermejo, *Polyhedron* 18 (1999) 2919–2929.
- [44] M.R. Mlahi, A. Negm, S.J. Azhari, M.M. Mostafa, *Appl. Organomet. Chem.* 28 (9) (2014) 712–719.
- [45] W. Linert, A. Taha, *J. Chem. Soc., Dalton Trans.* (1994) 1091–1095.
- [46] M. Govindarajan, S. Periandy, K. Carthigayen, *Spectrochim. Acta* 97 (2012) 411–422.
- [47] G.M. Abu, O.A. El-Reash, S.E. El-Gammal, A.H. Ghazy, Radwan, *Spectrochim. Acta Part A: Mol. Biomol. Spectrosc.* 104 (2013) 26–34.
- [48] R.G. Pearson, *J. Org. Chem.* 54 (1989) 1423–1430.
- [49] J. Padmanabhan, R. Parthasarathi, V. Subramanian, P. Chattaraj, *J. Phys. Chem. A* 111 (2007) 1358–1361.
- [50] R. Parthasarathi, J. Padmanabhan, U. Sarkar, B. Maiti, V. Subramanian, P.K. Chattaraj, *Internet Electron. J. Mol. Des.* 2 (2003) 798–813.
- [51] E. Scrocco, J. Tomasi, *Advances in Quantum Chemistry*, Academic Press, 1978, 115–193.
- [52] F.J. Luque, J.M. López, M. Orozco, *Theor. Chem. Acc.* 103 (2000) 343–345.
- [53] N. Okulik, A.H. Jubert, *Internet Electron. J. Mol. Des.* 4 (2005) 17–30.
- [54] P. Politzer, P.R. Laurence, K. Jayasuriya, *Environ. Health Perspect.* 61 (1985) 191–202.
- [55] E. Scrocco, J. Tomasi, *The Electrostatic Molecular Potential as a Tool for the Interpretation of Molecular Properties*, Springer, New concepts II, 1973, 95–170.